# Tetrahedral structures in the neuraminidases with special reference to influenza neuraminidase.

Donald G. Vanselow

*54 Greenways Road, Glen Waverley, Victoria 3150, Australia*

*Keywords*

Structure-function, Solution structure, Crystal structure, Symmetry, Constraint, Natural selection

*Running title* Tetrahedral structures in neuraminidases

Other address for correspondence
email: d.vanselow@UNSWalumni.com

ABSTRACT This report shows that a rearrangement of subunits from enzyme crystal structures, guided by symmetry and biophysical requirements, leads to a set of new tetrahedral quaternary structures for neuraminidases from viruses, bacteria and higher organisms. The new structures provide constraining environments for the active sites. In the case of viral neuraminidases, the locations of glycosylation sites and the points of attachment of the stalk or tether, together with the quality of steric and electrostatic fit, provide strong evidence that the tetrahedral structure is a native structure. For those neuraminidases from bacteria and the leech that have additional domains, the steric fit with the extra domains is also consistent with these being native structures. This discovery confirms the role of constraint in enzyme function and suggests the basic features to be expected in native structures of other enzymes and proteins.

## INTRODUCTION

In an earlier study of the theory of protein structure and function (1) it was argued that an enzyme must be able to constrain its active site. Using approximate calculations it was shown that the size of enzymes and the relative abundance of tetrameric forms were consistent with the provision of three-dimensional constraint. The theory predicts that the catalytic form of a tetrameric enzyme will be a tetrahedral arrangement of subunits with centrally located active sites. However, it was noted that the structures of proteins in crystals, on first inspection, showed no evidence of such arrangements.

In this study the aim was to explore alternative arrangements of subunits of a well-characterized family of enzymes composed of only one type of subunit. Some of the enzymes were reported to be homotetrameric, and some had been reported to have other degrees of association, based on associations seen in crystals. However, given that the assumption underlying the aim was that associations observed in crystals may not be the only or the principal native quaternary structures, all the enzymes were subjected to the same search for tetrameric forms. In general, a simultaneous four-molecule docking problem has a prohibitively large number of degrees of freedom and cannot be solved. However, consideration of the principles of evolution and Natural Selection as detailed in Appendix 1 suggests that a tetrahedral homotetramer should have D2 symmetry in its native state and the degrees of freedom become manageable. That is, by choosing a family of enzymes with only one type of subunit, the number of possible arrangements to be explored is greatly reduced. In addition, the viral enzymes have surface glycosylation sites in many cases, as well as a stalk or tether attachment, the locations of which further limit the possible quaternary structures. The neuraminidase superfamily (2) occurs across a diverse range of organisms. All members have in common a six-bladed “propeller” domain containing the active site, but may or may not have other loops or domains attached. The present study shows that, across the whole superfamily, there is a common tetrahedral arrangement of the propeller domains consistent with the locations of viral tethers and glycosylations as well as the locations of various attached auxiliary domains and loops.

The best-known neuraminidases, those from the influenza virus, are then studied in detail. Various experimental observations from the literature are explained in terms of the tetrahedral structure.

## METHODS

**Docking.** For each neuraminidase, the docking was primarily focused on the propeller domain. Sugar moieties or auxiliary domains attached to the propeller domain by a single freely-rotatable bond were considered to be mobile and their orientations in the crystals were discounted. In practice these appendages were deleted from the crystal structure files before docking was attempted. After docking, their points of attachment were checked for access to the solvent space. Loops or domains attached by two single bonds were considered to have a fixed orientation relative to the propeller and were not deleted before docking. Side chains of surface amino acids were considered to have a large degree of freedom of orientation and apparent clashes between them were given reduced weight in line with the practice of “soft docking” (3).

Docking was achieved by a computer-assisted manual trial-and-error method. To save time it was essential to use as much prior information as possible to narrow the search. Consequently, the docking was attempted first on the viral enzymes because of the relatively large number of surface features (tether and sugar side-chains) providing clues to the native orientation. After it became apparent that certain features of the propeller orientation were conserved, this orientation was used as the starting point for docking the bacterial and animal

neuraminidases. Initially the quality of fit in the tetramers was judged subjectively by the lack of empty space between subunits and the lack of steric clashes, especially backbone clashes. Subsequently methods were developed to quantify these features. In all, 11 neuraminidases were reassembled into tetrahedral structures.

The first neuraminidase reassembled was the influenza virus N2 type. The atomic coordinates of the crystal structure of this enzyme, are recorded in the Protein Data Base (PDB) with the identification code 1NN2 (4). Using the Swiss-PdbViewer (version 3.7) (5), the propeller axis (4) of a subunit of N2 neuraminidase was aligned along the (1, 1, 1) axis with the active site facing towards the origin. The (1, 1, 1) axis was chosen for convenience so that the two-fold rotational symmetry axes of the tetramer would be the x, y and z axes. The subunit was rotated about the (1, 1, 1) axis until Cysteine92 was as close as possible to the xy plane and the new coordinates were saved as a PDB file. The disulfide bond between Cys92 and Cys417 is the point of covalent attachment of the stalk or tether to the catalytic domain of the enzyme, as discussed in Appendix 2. For reasons discussed in Appendix 2, the most probable location of the point of attachment in the native structure would be on a plane containing two symmetry axes, and this was chosen to be the xy plane. The tether and the oligosaccharides attached to certain asparagine residues were then deleted from the PDB file. Three more copies of the relocated and edited N2 structure were then rotated 180° about the x, y and z axes respectively to generate a tetramer with D2 symmetry. The tetramer was then examined visually for quality of steric fit. The process was repeated several times with minor adjustments to the alignment of the propeller axis, the rotation about the (1, 1, 1) axis and the distance from the origin, to simultaneously optimize the three interfaces of each monomer with its neighbours. For convenience in describing relationships between subunits in the tetramer, the subunit aligned along the (1, 1, 1) axis was designated the A chain, while the copies rotated about the x, y and z axes were designated chains B, C and D respectively. Similar procedures and conventions were used for the docking of all 11 proteins.

**Recording of atomic coordinates** The atomic coordinates of the repositioned subunits are recorded in Appendix 3 as the translational and rotational operations that need to be applied to the respective original coordinates from the Protein Data Base to generate chain A of the tetrahedron.

**Description of propeller orientation.** For each protein, the axis of the propeller was defined as a line passing through the catalytically active tyrosine oxygen atom in the active site (6, 7), at the proximal end, and through the mid-point of the propeller blades at the distal end. This mid-point was the average of the coordinates of the alpha carbons of the six amino acids, one from each blade, nearest the axis at the distal end. The relevant amino acids are listed in Table 1. In addition to defining the propeller axis it was necessary to define the rotational orientation of the propeller about its axis. The catalytically active tyrosine described above has its phenolic oxygen on the propeller axis and its alpha carbon embedded in the sixth blade of the propeller in all the neuraminidases studied. Thus, the axis through the phenolic oxygen and the alpha carbon, the tyrosine axis, characterizes the rotational orientation of the propeller. The orientation of the tyrosine axis relative to the y axis was calculated by projecting both those axes onto a plane normal to the propeller axis and measuring the clockwise angle from the projected y axis to the projected tyrosine axis as viewed towards the origin. In practice this was done by translating the propeller so that its axis passed through the origin, then rotating it about y and then about z so that the propeller axis lay along the x axis. Thus the y axis became normal to the propeller axis and the slope of the tyrosine axis was calculated from the y and z coordinates of its alpha carbon.

**Measurement of effect of propeller rotation.** The docking results showed that the main differences in propeller orientation between species were in the rotational orientation about the propeller axis. Therefore, for three neuraminidases, other rotational orientations about the propeller axis were searched to confirm that the observed orientation of best fit was indeed unique with respect to that rotational degree of freedom. Angle of rotation was measured in the same way that propeller orientation, above, was measured. Lack of fit was measured at two levels of sensitivity; the number of atoms of any type apparently clashing, and the number of backbone atoms apparently clashing with other backbone atoms.

**Detection of apparent steric clashes** The in-built algorithm of RASMOL (8) was used for measuring the notional clashes generated by rotation of subunits about the propeller axis, with 3.0 Å separation between atomic centers taken as the threshold for a clash. In the detailed study of N2 and N9 neuraminidases, apparent steric clashes between subunits were detected using the CONTACT program of the CCP4 suite (9).

**Improved docking of N2 and N9 neuraminidases** To illustrate the ease with which the apparent clashes between side chains could be avoided in the proposed neuraminidase structures, selected rotamers from the Swiss PDBViewer library were substituted into the structure and found to largely eliminate the clashes. The substitutions in N2 were (rotamer library numbers in square brackets), Asp147 [6], His150 [8], Arg152 [18], Trp178 [9], Asp198 [3], Leu321 [1], Asp330 [2], Arg331 [12], Asn342 [15], Lys431 [7], and Thr455 [2]. In N9 the substitutions were Asn146 [2], His150 [7], Arg152 [18], Asn345 [10], Trp437 [3] and Gln455 [8]. Their coordinates in the A chain are included in the Supplementary Material in PDB format. The substitutions are not used elsewhere in this paper, except in the determination of buried surface areas detailed below.

**Measurement of accessible and buried surface areas** The AREAIMOL program of the CCP4 suite (9) was used to calculate the accessible surface areas of monomers and tetramers of N2 and N9 enzymes, with various probe sizes. From these measurements, the buried surface areas were calculated.

## RESULTS AND DISCUSSION

**Tetrahedral structures** Appendix 3 lists the transformations required to generate the A chain of each tetrahedron from the published coordinates in the Protein Data Base. The B, C and D chains can be generated by rotating the A chain 180° about the x, y and z axes respectively.

For N2 and N9, the only apparent steric clashes between main-chain atoms are between pairs of Asn342 residues on adjacent N2 chains and pairs of Gly343 on N9 chains. These apparent clashes could be relieved by displacements of about 1 Å. The position of Asn342 in the X-ray crystal structure of N2 is among the most uncertain (4), and Gly343 lies in a region of high mobility in the N9 crystal structure (10). The clashes are described as "apparent" because, if the subunits were brought together as described, the clashes would be avoided by very low energy conformational changes. Such low energy conformation changes have been observed in the surface residues of proteins crystallized with and without another protein, as discussed by Del Carpio Munoz et al. (3). Provision for the conformation changes is now incorporated in the techniques of "soft docking" (3, 11, 12). Del Carpio Munoz et al. (3) have allowed for the softness of protein surfaces by treating the outer 2.2 Å of protein surfaces as plastic materials able to freely interpenetrate each other.

Figure 1 is a computer graphic of the proposed N9 tetramer viewed down the y axis, showing the proximity of Cys92 residues to the xy plane. Figure 2 is a view down the z axis showing the self-complementarity of the interfaces.

The Influenza B enzyme crystal structure does not dock with itself quite as well as N2 and N9 do in the region of the active site, but it is otherwise similar to the other two influenza enzymes. There are no clashes between backbone atoms.

Parainfluenza-3 neuraminidase docks with itself very well and similarly shows no clashes between backbone atoms.

The parainfluenza-5 neuraminidase crystal structure lacks coordinates for residues 187-190. These amino acids would lie at the interface near the active site and therefore that part of the docking cannot be assessed. Apart from the missing residues, the docking is very good.

The crystal structure of the neuraminidase of Newcastle Disease Virus does not dock very well compared with the other viral neuraminidases. The tabulated transformations represent the best docking achievable without moving certain loops, especially residues 518-521. This loop has substantially different conformations in other PDB files of the same protein, but none of the files produces better docking.

Among the bacterial neuraminidases, Salmonella neuraminidase has only the propeller domain and it docks with itself fairly well, although some movement of residues 332-334 would improve the docking.

The Vibrio neuraminidase has two auxiliary domains in addition to the propeller domain. The N-terminal domain, joined to the propeller at residue 214, would clash in the tetrahedral structure but may be rotated out of the way. The second auxiliary domain is a loop from residues 354 to 539. It does not clash in the tetrahedral structure and contributes to the complementarity of docking.

Micromonospora viridifaciens has a neuraminidase with two C-terminal auxiliary domains. The first is joined to the propeller by residue 403 as well as a disulfide link from 351 to 405. The second is joined to the first through residue 503. This neuraminidase provides the most compelling visual evidence that the tetrahedral structures are natural, because of the complex shape of the monomer and the interlocking nature of the tetrahedral structure. Figure 3 is a view of the proposed tetramer viewed down the z axis. Comparison with Figure 2 shows that the docking of the propeller domains of chain A and chain D is the same in influenza and Micromonospora, despite the 86° difference in rotational orientation of the propellers (Table 1). This docking of the four central propeller domains of Micromonospora coincides with remarkably good docking of the other eight domains. The quality of the fit is further illustrated in Figure 4, which is a view down the x axis of the Micromonospora tetramer. For Micromonospora, the docking was initially carried out on the propeller domains alone and it was only subsequently discovered that the same transformation produced very good docking of all domains.

The Leech neuraminidase has an N-terminal auxiliary domain joined to the propeller through Glycine277. This domain extensively overlaps with the propeller domain of symmetry-related subunits across the x axis, but can be rotated out of the way. There is also an auxiliary loop domain from residue 406 to 504 that docks well with its symmetry-related counterpart across the z axis. These domains contribute to the occlusion of the active site.

The Human neuraminidase has no auxiliary domains and docks well across the x and y axes. However a large number of residues near the z axis could not be located by X-ray crystallography and so the docking near the active site cannot be assessed.

**Geometry of the tetrahedral structures** The locations of the phenolic groups of the reported catalytic tyrosines are tabulated in Table 2. The location is highly conserved; all examples occur within 5 Å of the average position, approximately represented by the enzyme from parainfluenza virus-3. According to the theory of constraint (1) the catalytic site would have to be located precisely where compressive stress was optimal. This would account for

the high degree of conservation. Another feature that is highly conserved is the propeller axis. The gradients and intercepts of the equations to the axes are listed in Table 1, showing little variation. A feature that is not conserved across the superfamily is the rotational orientation of the propeller about its axis. These values are also listed in Table 1. It is estimated that they are meaningful within a range of ± 5 degrees, based on Figure 5. There appear to be groupings based on genetic relatedness of the source organisms. In the case of the viruses, the orientation of the propeller is strongly linked to the need for the tether attachment to be as close as possible to the xy plane, but it cannot be said which phenomenon is driving the other.

**Locations of tether attachments** For four of the viral enzymes, the tether attaches to embedded protein chain by a disulfide bridge. These cases are listed in Table 3, together with the coordinates of the alpha carbon of the tethered (N-terminal) cysteine. It can be seen that all such points of attachment are within 11 Å of the xy plane and located more than 39 Å from the origin, as expected if the tethers are to be able to reach the virus surface without obstruction.

**Steric clashes** During docking, clashes between side-chains of a small number of amino acids were tolerated, as changes to side-chain orientation involve negligible energy. The examples of the N2 and N9 enzymes are detailed in the Methods section. A very small number of clashes between backbone atoms were also tolerated as these could be relieved by small changes in chain configuration.

**Effect of rotation about propeller axis on steric clashes** Of the six degrees of freedom available during symmetrical docking, variations of most of them would have predictable effects on steric clashes. Only one degree of freedom seems to be variable in nature, as shown by differences between species, and that is rotation about the propeller axis. This rotation was chosen to illustrate the energy minimum, represented by minimum steric clashes, corresponding to the docked structures. One viral, one bacterial and one animal enzyme were chosen for this study. Close to the optimally docked structure, both backbone and sidechain clashes were recorded, but for rotations more than 30° away from the optimum, only backbone clashes were recorded. The results are graphed in Figure 5. For Vibrio and Leech neuraminidases there is a unique minimum of clashes, both backbone and sidechain, corresponding to the optimally docked "native" structure. Note that for Vibrio and Leech, the N-terminal domain was excluded from the measurements as it is assumed to be incorrectly orientated in the crystal as discussed above. For influenza type N9, there is a sharp minimum of clashes at the "native" orientation, but also a broad minimum 120° away. Inspection of the latter tetramer showed that the subunits were in an orientation where there was a large central cavity and sparse circumferential contacts between subunits. That is, there was very little buried surface area. While this orientation would have low energy with respect to steric clashes, it would have high energy because of the small buried area.

**Residual internal crevices and buried accessible surface area**. Apart from the lack of high-energy steric clashes, a measure of the quality of fit is the size and shape of the remaining inter-subunit crevices. According to the theory of constraint (1), the central core of the catalytically active tetrahedron should be tightly packed, except where space has been left by the absence of reactants or products. The residual crevices resulting from the imperfection of bringing the crystal structures of the subunits together were characterized by measuring the buried accessible surface area of the N2 and N9 tetrahedra as a function of the radius of the probe used to measure the surface areas. To reduce errors arising from the apparent steric overlap of side-chains, the rotamer substitutions listed in Methods were incorporated into the structures for these measurements. The results for the tetrahedra are compared with the square crystal structures in Figure 6. It can be seen that the residual crevices in the tetrahedra

are of the order of 2 to 3 Å across, a distance comparable to the known uncertainty in the shape of a protein surface (3). It is assumed that full relaxation of the tetrahedral structures would completely eliminate the residual crevices. Such full relaxation has not been attempted in this study, but it can be inferred from the above, that an overall movement of each subunit of only 1-2 Å towards the origin would allow elimination of all residual crevices. Since some parts of the subunits are already in contact before relaxation, some slight flexing of the whole subunit structure would have to be included in the relaxation process.

Buried surface area is often used as a crude measure of the hydrophobic interaction energy between proteins. A better measure would take account of the hydrophobic interaction that occurs even when surfaces are not in contact (1). For the present purposes, the buried surface areas measured by the AREAIMOL program of the CCP4 suite were compared between the proposed native tetramers and the recorded crystalline tetramers.

In Figure 6, the gradual increase of buried surface area of crystal structures with probe size is approximately what would be expected for a cylinder of 25 Å radius abutting a larger structure. It can be seen that, apart from the steep change of buried surface area caused by residual crevices, the tetrahedral structures result in slightly larger buried surface areas than in the crystal structures. The conclusion that can be reached is that, even using this crude measure of interaction energy, the proposed native structures are as likely to exist in solution as the crystalline structures are.

**Locations of glycosylated asparagines** Many animal proteins, and hence animal virus proteins, have oligosaccharides attached through the amide groups of surface asparagine residues that are part of a specific sequence (13) or sequon (14). As a result of glycosylation experiments it is generally accepted that all the appropriate sequons in a protein are able to be glycosylated except in cases where the protein is synthesized without any glycosylation, or the glycosylation system of the cell is defective, or there is a protein structural factor preventing glycosylation (14). Oligosaccharide side chains have never been found inside a protein structure. Because of their hydrophilic nature, it would seem energetically unfavourable.

For the N2 subunit, there are three widely spaced glycosylated sites (asparagines 146, 200 and 234) (4), all of which occur on the outside of the proposed arrangement or at the borderline between outside and inside. Asn146 is borderline, as only low energy side-chain rotations are needed to give the amide group clear access to the exterior. This glycosylation site is circled in Figure 6.

For N9 there is one demonstrated glycosylated site at Asn199 (10) (listed as Asn200 in the PDB file), which is on the outside.

For Influenza B (Lee) there is one demonstrated glycosylation site at Asn284 according to the PDB file, 1inf.pdb (15), and this site is on the outside.

The parainfluenza-3 enzyme has three glycosylated sites (16). Asn308 and Asn351 are on the outside while Asn523 lies in the cleft where three domains meet.

The parainfluenza-5 enzyme also has three glycosylated sites (17), with Asn139 and Asn267 on the outside and Asn504 borderline.

Lastly, amongst the current collection of viral neuraminidase structures, the Newcastle Disease Virus has four glycosylated sites (18) of which three are included in the PDB file. Asn341 is borderline while Asn433 and Asn481 are on the outside.

In all, there are 14 glycosylated sites in this collection of virus neuraminidase structures and all are compatible with the tetrahedral structures, with the possible exception of Asn523 of parainfluenza-3.

**Locations of unoccupied potential glycosylation sites** In the case of N2 neuraminidase, there is a potential glycosylation site (Asn402) on the subunit surface that is not glycosylated (4). With the proposed tetrahedral subunit arrangement, Asn402 is internal and it might be supposed that this is the reason that Asn402 is not glycosylated. However, the Newcastle Disease Virus neuraminidase has unoccupied potential glycosylation sites at Asn508 and Asn538 (18) and both these sites are on the outside of the proposed tetrahedral structure. It is therefore not possible to draw any meaning from the location of unglycosylated sites.

**Location of the hemagglutinin site on N9 neuraminidase** Apart from its neuraminidase ability, the N9 enzyme has the ability to agglutinate red blood cells (19) by binding their surface polymers. If this binding is brought about by constraint (1), such a high affinity binding site should be located inside the tetrahedron, just as the catalytic site is. Studies of laboratory variants (19) show that the amino acids important for binding are 368-370, 372, 400 and 432 (N2 numbering), all of which are located inside the proposed tetrahedral structure.

**Steric and electrostatic self-complementarity of the interfaces of influenza type N2 neuraminidase** Figure 7 is a map of the three interfaces that chain A of N2 has with its neighbouring chains. The three interfaces have been rotated into the plane of the page. The conformation of each amino acid side-chain is shown exactly as in the crystal structure; no rotamers have been substituted into the structure. Each interface stretches between two pseudo-threefold axes, and the interfaces with chains B, C and D are centered on the x, y and z axes respectively. On this map, amino acid residues lying along a pseudo-threefold axis appear in both of the interfaces meeting at that axis, but are viewed from different angles. An N-acetylglucosamine mannose disaccharide has been included in the AD interface to show where it is thought most likely that an oligosaccharide substrate (e.g. sialic acid - galactose - N-acetylglucosamine - mannose - mannose (13)) would project into the catalytic cleft. It has been fitted into a narrow channel that connects the interior of the catalytic cleft to the surrounding medium at the point where three subunits meet. There are, of course, four symmetry-related channels in the tetrahedron, but only one is shown occupied. The coordinates of the disaccharide are included in the Supplementary Material in PDB format. The reducing end of the mannose is located outside the enzyme and the non-reducing end of N-acetylglucosamine is located inside the catalytic cleft where it would connect through a galactose residue to the terminal sialic acid. Amino acid residues 368 and 369 lie at the center and appear in all three interfaces.

For self-complementarity, the half of each interface lying to the left of its central axis should be complementary to the half lying to the right. On the AB and AC interfaces, the steric features are no bigger than the uncertainty in orientation of side chains, so these interfaces provide no evidence for or against steric self-complementarity. However, the AD interface contains the catalytic cleft on one side of the z axis and a corresponding knob of large amino acids (residues 430-437) on the other side, as marked on the map. This knob partly protrudes into the cleft and would protrude even further if the subunits were relaxed together. There are differences in the shapes of the cleft and the knob, but these are comparable to the uncertainty in orientation of side-chains. The cleft and knob features are evidence of self-complementarity and occur in similar positions in both N2 and N9 enzymes.

There are a number of charged groups in the interfaces and these could provide strong evidence of self-complementarity if we knew what to look for. Buried charged groups, even when paired as a salt bridge, are destabilizing (20, 21), although uncompensated charges are much more destabilizing than bridged charges. On theoretical grounds, the force-separation relationship of a salt bridge across an interface is expected to be repulsive while water is

being displaced from the charges by close approach of the protein interfaces (Born repulsion), but attractive once water has been displaced. This kind of force-separation relationship could be important for enzyme function (1). On theoretical grounds, a close pair of salt bridges, or a quadrupole, would be expected to be less destabilizing than two separate salt bridges and, extending this line of reasoning, a zone of ionic structure would be still less unstable (20). Various arrangements of charged groups could be employed to produce a functional force-separation relationship and these considerations do not necessarily lead to an expectation of charge self-complementarity across the interfaces. On the other hand, when we consider possible lateral sliding of the interfaces, an argument for self-complementarity becomes clear. Assuming that lateral sliding of the interfaces would produce a non-functional structure, and that thermal motion is continually disturbing the structure, it is reasonable to expect that Natural Selection would have provided surface features that oppose and correct any sliding. The steric features described above are an example. Under sliding motion, there is no change in the dielectric constant of the environment of charges and therefore no doubt that opposite charges are strongly attracted. Hendsch and Tidor (20) proposed that the role of buried salt bridges is to produce structural specificity. Therefore it is reasonable to expect that a native structure will exhibit a number of examples of opposite charges in contact with each other across the interfaces.

The AB interface of N2 contains two sets of two symmetry-related zones of ionic structure with contributions from both subunits. It appears that the signs and locations of the charges are such as to provide nearly equal numbers and even distributions of positive and negative charges. The two different zones are Glu433, Arg428 and Asp460 of chain A with Arg331 of chain B, and Arg327, Asp329, Asp330, Arg364, Glu375, Arg394 of chain A with Asp401 and Asp399 of chain B. Because of uncertainty about the side-chain orientation of Asp329, it is not clear whether this zone is contiguous with the central ionic zone comprising the four sets of lys368 and asp369 pairs.

The AC interface contains only two sets of pairs of opposite charges. One pair, Asp339 and Lys296, is exposed to the solvent and therefore in a high dielectric environment. This would reduce the force of attraction. The second pair, Glu343 and Arg344, have their charged groups widely separated in the crystal structure although their alpha carbons are adjacent in the chain. Arg344 in particular seems free to adopt many other rotameric structures and it is not clear why its charged group is located where it is in the crystal structure. If the subunits were brought together as proposed, this separation of charges would become very unfavourable and it is likely that Glu343 and Arg344 would form a salt bridge and possibly a quadrupole with their symmetry-related pair. It is worth recalling that the adjacent Asn342 is involved in an apparent steric clash with its symmetry-related counterpart. Therefore, bringing the subunits together as proposed would affect the locations or orientations of the sequence 342, 343 and 344. However, this argument is somewhat speculative and it is conceded that this part of the crystal structure does not provide strong evidence for electrostatic self-complementarity.

The AD interface contains the catalytic cleft and the 430-437 knob. The large number of charged groups in these two features (the knob has one negative and three positive charges) have not been included in the map as they doubtless have substrate binding and catalytic functions and may not conform to self-complementarity. Furthermore, it is difficult to represent these features on a two-dimensional map. Outside of these features, there are a number of examples of electrostatic self-complementarity. The C-terminus carboxyl group of Ile469 on one subunit contributes to a zone of ionic structure with Arg224, Lys199, Asp198, and Arg152 on the other subunit. Asp197 and Lys143 form an interfacial salt bridge in a

region exposed to solvent. Therefore they would be weakly attracted. The two symmetry-related pairs of His150 and Asp147 form a quadrupole in the center of the interface. This would be strongly attractive. In other strains of influenza, other residues are present at position 147 and it is not clear which negatively charged amino acid, if any, is compensated by His150 in these cases. Because the pKa of histidine is close to physiological pH, burial of an uncompensated histidine involves loss of the charge on the histidine and very little energy change. Therefore an uncompensated histidine at an interface would provide no significant barrier to intersubunit contact.

**A destabilized mutant of influenza type N9 neuraminidase** McKimm-Breschkin et al. (22) and Colacino et al. (23) discussed a mutant of N9 neuraminidase in which Glu119 in the catalytic cleft was mutated to Gly119. This mutation had the effect of relieving inhibition of the enzyme by the sialic acid analog, 4-Guanidino-Neu5Ac2en. It also had the effect of causing progressive dissociation of tetramers into monomers (23) and the loss of susceptibility to binding by the monoclonal antibody NC10 (22). As the Glu119 charged group is remote from any of the interfaces found in the crystal structure, there was some difficulty in explaining its destabilizing effect. In the crystal, the nearest part of a neighbouring subunit is Trp456, 12.65 Å away, atom center to atom center, through protein structure. McKimm-Breschkin et al. (22) suggested the destabilisation was part of a general denaturation brought about by an entropy effect associated with glycine residues. Colacino et al. (23) suggested that the destabilisation resulted from mechanical transmission of a change of conformation through the protein structure to the interface. However, examination of the currently proposed native structure of N9 provides a more plausible explanation. As the structure is presented here, the charged group of Glu119 is only 7.1 Å away from the 430-437 knob of the adjacent subunit across a crevice. Since a 3.6 Å separation of atom centers constitutes contact, this means that Glu119 is only 3.5 Å away from intersubunit contact as the structure is presented. If the proposed structure were relaxed together, it seems likely that each subunit could move 1 -2 Å closer to the origin, as discussed earlier, and Glu119 could be in contact with the 430-437 knob of the adjacent subunit. In N9, the 430-437 knob has an overall single positive charge. Therefore, a mutation that removed the negative charge at position 119 could easily bring about destabilisation of the tetramer. It is also possible to propose an explanation for the fact that tetramers of the mutant enzyme were formed in the first place. It could be that molecules, such as oligosaccharides, bound within the catalytic cleft affected the stability of the mutant tetramer. Storage or processing conditions that progressively changed the nature of the bound molecules could have resulted in progressive destabilisation of tetramers that had been stable at the time of synthesis.

**The occurrence of square arrangements in crystals and electron micrographs of influenza neuraminidase** Adsorption is a process common to electron microscopy and crystal growth. In production of protein crystals, the first step is nucleation. After that, further protein molecules adsorb to the nascent or growing crystal, taking up ordered orientations that allow an X-ray diffraction pattern to be recorded. In transmission electron microscopy, the proteins are first adsorbed onto a polymer film suspended across a copper grid. They are then dried and stained. Because the proteins are not closely packed, the proteins can take up orientations that are random in two dimensions (the plane of the polymer) but tend to be ordered in the other dimension because of interfacial forces.

When influenza virus neuraminidase is freed from the virus with detergent and fixed onto a surface for electron microscopy, the individual catalytic subunits dissociate while the anchor regions at the N-terminal of the tether remain associated, giving a characteristic "rosette" adsorbed flat against the polymer surface (19). However, if the enzyme is freed by

enzymic cleavage of the tethers rather than detergent, a square packed arrangement of subunits is observed (23) and, because of the interfacial forces, all the squares lie flat against the polymer film. The uniform occurrence of square structures has been tentatively taken to support the idea, also suggested by the crystal structure, that the square arrangement is the native conformation (19). However, given that the method of specimen preparation for electron microscopy involves an adsorption step similar to the process of crystal growth, the occurrence of squares is not a fully independent observation. Indeed, it is well recognized by electron microscopists that the adsorption step, together with the drying and staining steps in that technique, usually generates artefacts (24). Therefore the absence of tetrahedral forms in electron micrographs does not preclude the possibility that tetrahedral forms occur in solution.

**Comparison with the theoretical model structure** While the discovery of these tetrahedral arrangements confirms the applicability of constraint theory to this enzyme family, there are differences from the model structure (1).

Firstly, the radius of the region of high compression (1), as shown by contact between subunits, was 25 Å in this real enzyme whereas the simple model predicted it only needed to be at least 6.3 Å. Perhaps this is because the substrate is particularly large in this case.

Secondly, the real enzyme is far from spherical. Whereas the model involved segments shaped like flattened quarterspheres, the real enzymes have segments consisting of lobes protruding into the aqueous environment. This difference is very important. It was assumed that the protein material of the model enzyme had sufficient cohesive strength to redirect inter-subunit hydrophobic attraction into centrally focussed compressive stress. However, hydrophobic interactions are merely a manifestation of the surface excess chemical potential of surrounding water (1) and therefore the hydrophobic contribution to the strength of a protein subunit depends inversely on its proximity to other subunits. The structure of the real enzyme suggests that this factor dictates a relatively large distance between segments, of the order of 25 Å rather than the 6 Å assumed in the model (1). However, the presence of auxiliary domains in many of the neuraminidase enzymes would tend to reduce the average distance between segments and it is unclear what advantage or function they might have. They might produce subtle variations in the pattern of compressive stress inside the enzyme.

**Implications for development of anti- influenza drugs and research into influenza antigenicity.** The X-ray structure of the catalytic cleft of neuraminidase has been used to help in the design of inhibitors of the enzyme as a treatment for influenza (25). The inhibitors are analogs of sialic acid, one of the products of the enzyme. The present work suggests that the X-ray structure of the cleft is not complete in that it lacks the contribution of the 430-437 knob. However, the X-ray structure probably resembles quite closely the form of the catalytic cleft that initially encounters the substrate; that is, the cleft is open to the surrounding medium and relatively unconstrained. It may be that the X-ray structure has been quite helpful in designing the analogs, but a more accurate model of the catalytic cleft in action could lead to further possible designs of inhibitors, potentially with more efficacy as treatments.

It also seems that research into the antigenicity of influenza has been unnecessarily narrowed by the belief that the square arrangement of subunits was the native form. Parts of the enzyme surface were considered inaccessible to antibodies (19) and work with monoclonal antibodies and escape mutants has been interpreted on the assumption that the "top" surface of the square was accessible to antibodies (19, 20). The interaction between an

antigen and antibody can be disrupted by a mutation within the epitope on the antigen, or at some other site that disrupts the epitope. This suggests that, for epitopes lying partly on one subunit and partly on another, a mutation causing dissociation of the subunits would disrupt the antibody- antigen interaction. This appears to be the simplest explanation for the observations of McKimm-Breschkin et al. (22) and Colacino et al. (23) concerning a mutant of N9 neuraminidase that gradually lost enzyme activity and susceptibility to a monoclonal antibody at the same time. These results are discussed in an earlier paragraph. Although this mutant was not isolated by antibody challenge it had the property of resistance to the N10 monoclonal antibody, as if it was an escape mutant, and can serve as a model for most escape mutants studied to date.

It happens that only those antibodies that inhibit neuraminidase activity have produced escape mutants (19, 20) and the currently proposed model of native neuraminidase suggests that such antibodies would bind to the exterior of the tetramer at the pseudo-threefold axis and block access of substrate. It is therefore expected that binding of such antibodies would be prevented by any mutation that caused subunit dissociation, such as reported by Colacino et al. (23). Examination of the locations of escape mutants (19) on the proposed native interface shows that, for N2, 8 of the 9 sites are within the interface, 7 of them within 15 Å of the origin, and 5 of those lying along the pseudo-threefold axes. The two other sites close to the origin and not on the pseudo-threefold axes are near the centers of the AC and AD interfaces. For N9 (19), all of the 8 sites are close to the origin, many also lying on the pseudo-threefold axes. For N8 (26), 7 of the 8 sites would be close to the origin, but most of these sites would not be close to the pseudo-threefold axes. The eighth site lies on the bottom of the square arrangement and on the exterior of the proposed tetrahedral arrangement and is not considered to have a role in reducing susceptibility to the antibody (26). It seems that all but one or two of the escape mutants must have acted by destabilizing the tetramer and reducing the amount of intact antigen on the virus. If this is so, the locations of these mutations do not define the epitopes of the antibodies that selected for them. There appear to be differences between the neuraminidase types with respect to the regions where mutations are most likely to cause dissociation. For N2, the susceptible region appears to be the pseudo-threefold axes. For N9, the susceptible region is close to the origin and close to a pseudo-threefold axis. For N8, the pseudo-threefold axes appear to be not susceptible and the effective mutations are located elsewhere. These sites of vulnerability could be potential sites for action by new anti-influenza drugs, as could the site where substrate enters the catalytic cleft.

Saito et al. (26) measured the effect of antibody concentration on the neuraminidase activity of their N8 escape mutant viruses. The neuraminidase assay did not allow comparison of the relative activity of different virus preparations. The results showed that there was some enzyme activity remaining in the escape mutants, but not how they compared with the parent strain. Only a study similar to that conducted by Colacino et al. (23) could show whether the escape mutant enzymes were largely dissociated.

**Implications for X-ray crystallography of proteins** X-ray crystallography of proteins is a series of three procedures, each with different precision and accuracy characteristics. The aim is to represent a native structure of a protein as a set of spatial coordinates for each atom in the protein. The first procedure is the production of a crystal of the protein, which will be discussed later. The second procedure is the actual X-ray crystallography step, in which a map of electron density in a crystal is determined by a well-understood physical phenomenon able to be measured with high precision and high reproducibility with suitable crystals. The third procedure introduces further information about the sequence of the protein and

limitations on the steric arrangements deduced from other experiments. Without the sequence, the chemical elements associated with each center of electron density would not be known. Because this procedure takes the form of numerical modelling, there is no limit on the amount of precision it can generate and, because of the extra information brought into the calculations from other measurements, it also considerably increases the accuracy of the X-ray work.

However, the accuracy of the crystallisation step is problematic. Each protein crystallisation is a unique technical problem. The process of crystallisation is a combination of complex chemical interactions, each of them poorly understood, and it is not possible to say from first principles to what extent any crystal structure will reflect a structure in solution. Once a crystal has been produced and its atomic coordinates determined with high precision, there is no other technique that can be applied to a protein solution with enough precision to enable the accuracy of the crystallisation to be measured, except in rather broad terms. For larger proteins beyond the reach of nuclear magnetic resonance methods, there have been only very imprecise and scanty data with which to compare the crystal structures, until now.

The work described in this report now allows the crystal structure of neuraminidases to be measured against themselves and the accuracy of these particular crystallisations can be estimated. The native conformation of neuraminidase was reconstructed by introducing further information about biological and biophysical principles and discarding less than 1% of the information contained in the PDB file. The discarded information was the symmetry information, the location of the origin and the orientations of certain surface amino acids. It could be said that the crystallisation of neuraminidase was of the order of 1% inaccurate in terms of transmitting information about structure. Because each protein crystallisation is unique, it may not be possible to extrapolate that estimate of inaccuracy to another protein, but it seems there is only a low level of inaccuracy. Unfortunately, the inaccurate information has affected our knowledge of the overall shape of the proteins and locations of interfaces and this has held back the understanding of function.

## REFERENCES

(1) Vanselow, D G. 2002. Role of constraint in catalysis and high-affinity binding by proteins, Biophys. J. 82: 2293–2303.

(2) Roggentin, P., R. Schauer, L. L. Hoyer, E. R. Vimr. 1993. The sialidase superfamily and its spread by horizontal gene transfer. Mol. Microbiol. 9: 915-921.

(3) Del Carpio Munoz, C. A., T. Peissker, A. Yoshimori, E. Ichiishi. 2003. Docking unbound proteins with MIAX: a novel algorithm for protein-protein soft docking. Genome Informatics 14: 238-249.

(4) Varghese, J N., P. M. Colman. 1991. Three-dimensional structure of the neuraminidase of influenza virus A/Tokyo/3/67 at 2.2 Å resolution. J. Mol. Biol. 221: 473–486.

(5) Guex, N., M. C. Peitsch. 1997. Swiss-Model and the Swiss-PdbViewer: An environment for comparative protein modeling. Electrophoresis 18: 2714–2723. http://www.expasy.org/spdbv/ (2003)

(6) Chavaz, L. M. G., C. Tringali, P. Fusi, B. Venerando, G. Tettamanti, R. Kato, E. Monti, S. Wakatsuki. 2005. Crystal structure of the human cytosolic sialidase Neu2. J. Biol. Chem. 280: 469-475.

(7) Crennell, S. J., E. F. Garman, , W. G. Laver, E. R. Vimr, G. L. Taylor. 1993. Crystal structure of a bacterial sialidase (from Salmonella typhimurium LT2) shows the same fold as an influenza virus neuraminidase. Proc. Natl. Acad. Sci. USA 90: 9852-9856.

(8) RASMOL version 2.6-ucb. 1995. Written by Roger Sayle, Glaxo Wellcome Research and Development, Stevenage, Hertfordshire, U.K. and enhanced by the University of California, Berkley.

(9) Collaborative Computational Project, Number 4. 1994. The CCP4 suite: programs for protein crystallography. Acta Cryst. D50: 760–763.

(10) Tulip, W. R., J. N. Varghese, A. T. Baker, A. van Donkelaar, W. G. Laver, R. G. Webster, P. M. Colman. 1991. Refined atomic structures of N9 subtype influenza virus neuraminidase and escape mutants. J. Mol. Biol. 221: 487–497.

(11) Waszkowycz, B. 2002. Structure-based approaches to drug design and virtual screening. Curr. Opin. Drug Discovery Dev. 5: 407-413.

(12) Carlson, H. A. 2002. Protein flexibility is an important component of structure-based drug discovery. Curr. Pharm. Des. 8: 1571-1578.

(13) Hubbard, S. C., R. J. Ivatt. 1981. Synthesis and processing of asparagine-linked oligosaccharides. Ann. Rev. Biochem. 50: 555–583.

(14) Mills, K., P. B. Mills, P. T. Clayton, N. Mian, A. W. Johnson, B. G. Winchester. 2003. The underglycosylation of plasma $\alpha_1$-antitrypsin in congenital disorders of glycosylation type 1 is not random. Glycobiology 13: 73-85.

(15) Sudbeck, E. A., M. J. Jedrzejas, S. Singh, W. J. Brouillette, G. M. Air, W. G. Laver, Y. S. Babu, S. Bantia, P. Chand, N. Chu, J. A. Montgomery, D. A. Walsh, M. Luo. 1997. Guanidinobenzoic acid inhibitors of influenza virus neuraminidase. J. Mol. Biol. 267: 584-594.

(16) Lawrence, M. C., N. A. Borg, V. A. Streltsov, P. A. Pilling, V. C. Epa1, J. N. Varghese, J. L. McKimm-Breschkin, P. M. Colman. 2004. Structure of the haemagglutinin-neuraminidase from human parainfluenza virus type III. J. Mol. Biol. 335: 1343-1357.

(17) Yuan, P., T. B. Thompson, B. A. Wurzburg, R. G. Paterson, R. A. Lamb, T. S. Jardetzky. 2005. Structural studies of the parainfluenza virus 5 hemagglutinin-neuraminidase tetramer in complex with its receptor, sialyllactose. Structure 13: 803-815.

(18) Panda, A., S. Elankumaran, S. Krishnamurthy, Z. Huang, and S. K. Samal. 2004. Loss of N-linked glycosylation from the hemagglutinin-neuraminidase protein alters virulence of Newcastle disease virus. J. Virol. 78: 4965-4975.

(19) Colman, P. M., Neuraminidase enzyme and antigen. In The Influenza Viruses. R. M. Krug, editor. Plenum Press, New York. 175–218.

(20) Hendsch, Z. S., B. Tidor. 1994. Do salt bridges stabilize proteins? A continuum electrostatic analysis. Protein Sci. 3: 211-226.

(21) Chong, L. T., S. E. Dempster, Z. S. Hendsch, L-P. Lee, B. Tidor. 1998. Computation of electrostatic complements to proteins: a case of charge stabilized binding. Protein Sci. 7: 206-210.

(22) McKimm-Breschkin, J. L., M. McDonald, T. J. Blick, P. M. Colman. 1996. Mutation in the influenza virus neuraminidase gene resulting in decreased sensitivity to the neuraminidase inhibitor 4-guanidino-Neu5Ac2en leads to instability of the enzyme. Virology 225: 240–242.

(23) Colacino, J. M., N. Y. Chirgadze, E. Garman, K. G. Murti, R. J. Loncharich, A. J. Baxter, K. A. Staschke, W. G. Laver. 1997. A single sequence change destabilizes the influenza virus neuraminidase tetramer. Virology 236: 66–75.

(24) Adrian, M., J. Dubochet, J Lepault, A. W. McDowall. 1984. Cryo-electron microscopy of viruses. Nature 308: 32–36.

(25) von Itzstein, M., J. C. Dyason, S. W. Oliver, H. F. White, W. Y. Wu, G. B. Kok, M. S. Pegg. 1996. A study of the active site of influenza virus sialidase: an approach to the rational design of novel anti-influenza drugs. J. Med. Chem. 39: 388-391.

(26) Saito, T., G. Taylor, W. G. Laver, Y. Kawaoka, R. G. Webster. 1994. Antigenicity of the N8 influenza A virus neuraminidase: existence of an epitope at the subunit interface of the neuraminidase. J. Virol. 68: 1790-1796.

(27) Varghese, J. N., V. C. Epa, P. M. Colman. 1995. Three-dimensional structure of the complex of 4-guanidino-Neu5Ac2en and influenza virus neuraminidase. Protein Sci. 4: 1081–1087.

(28) Zaitsev, V., M. von Itzstein, D. Groves, M. Kiefel, T. Takimoto, A. Portner, G. Taylor. 2004. Second sialic acid binding site in Newcastle disease virus hemagglutinin-neuraminidase: implications for fusion. J. Virol. 78: 3733-3741.

(29) Crennell, S. J., E. F. Garman, C. Philippon, A. Vasella, W. G. Laver, E. R. Vimr, G. L. Taylor. 1996. The structures of Salmonella typhimurium LT2 neuraminidase and its complexes with three inhibitors at high resolution. J. Mol. Biol. 259: 264-280.

(30) Crennell, S., E. Garman, G. Laver, E. Vimr, G. Taylor. 1994. Crystal structure of Vibrio cholerae neuraminidase reveals dual lectin-like domains in addition to the catalytic domain. Structure 2: 535-544.

(31) Watson, J. N., S. Newstead, V. Dookhun, G. Taylor, A. J. Bennet. 2004. Contribution of the active site aspartic acid to catalysis in the bacterial neuraminidase from Micromonospora viridifaciens. FEBS Lett. 577: 265-269.

(32) Luo, Y., S. C. Li, M. Y. Chou, Y. T. Li, and M. Luo. 1998. The crystal structure of an intramolecular trans-sialidase with a NeuAcα2→3Gal specificity. Structure 6: 521-530.

**TABLE 1 Geometrical parameters in the tetrahedral structures.**

| Enzyme type | Propeller axis | | | | | | Tyrosine axis |
|---|---|---|---|---|---|---|---|
| | Distal end | Proximal end | Equations to axis | | | | |
| | Residue Nos. | Tyr No. | y=mx+c | | z=nx+d | | *Angle from y |
| | | | m | c (Å) | n | d (Å) | |
| Influenza N2 | 126, 184, 233, 284, 356, 413 | 406 | 0.64 | 5.1 | 0.01 | 17.0 | 152° |
| Influenza N9 | 126, 185, 233, 283, 356, 412 | 406 | 0.62 | 4.9 | 0.05 | 16.6 | 151° |
| Influenza B (Lee) | 123, 185, 232, 283, 356, 416 | 409 | 0.57 | 3.7 | -0.01 | 19.5 | 150° |
| Human Parainfluenza virus-3 | 198, 260, 328, 415, 484, 536 | 530 | 0.56 | 6.1 | -0.09 | 18.0 | 107° |
| Simian Parainfluenza virus-5 | 170, 231, 295, 397, 469, 529 | 523 | 0.50 | 7.0 | -0.16 | 19.7 | 116° |
| Newcastle disease virus | 182, 242, 306, 407, 475, 535 | 526 | 0.50 | 4.2 | -0.31 | 20.3 | 95° |
| Salmonella typhimurium | 45, 106, 185, 236, 288, 349 | 342 | 0.69 | 9.7 | -0.14 | 21.4 | 81° |
| Vibrio cholerae | 232, 299, 555, 626, 689, 747 | 740 | 0.87 | 5.1 | -0.22 | 17.6 | 73° |
| Micromonospora viridifaciens. | 78, 107, 138, 213, 320, 377 | 370 | 0.67 | 8.1 | -0.27 | 17.7 | 68° |
| Leech | 301, 382, 548, 602, 653, 718 | 713 | 1.09 | 4.6 | -0.05 | 17.6 | 127° |
| Human | 29, 93, 168, 225, 280, 341 | 334 | 0.77 | 3.5 | -0.37 | 21.0 | 126° |

*clockwise viewed towards origin

**TABLE 2 Locations of active phenolic oxygens in the tetrahedral structures.**

| Enzyme type | Tyr No. | Coordinates (Å) | | |
|---|---|---|---|---|
| | | x | y | z |
| Influenza N2 | 406 | 8.0 | 10.2 | 17.1 |
| Influenza N9 | 406 | 8.2 | 10.0 | 17.0 |
| Influenza B (Lee) | 409 | 8.6 | 8.7 | 19.4 |
| Human Parainfluenza virus-3 | 530 | 7.5 | 10.3 | 17.3 |
| Simian Parainfluenza virus-5 | 523 | 7.1 | 10.5 | 18.6 |
| Newcastle disease virus | 526 | 9.9 | 9.2 | 17.2 |
| Salmonella typhimurium | 342 | 4.5 | 12.9 | 20.8 |
| Vibrio cholerae | 740 | 5.9 | 10.3 | 16.4 |
| Micromonospora viridifaciens. | 370 | 3.0 | 10.1 | 16.9 |
| Leech | 713 | 8.2 | 13.6 | 17.2 |
| Human | 334 | 7.2 | 9.1 | 18.3 |

**TABLE 3 Locations of tether attachments in the tetrahedral structures.**

| Enzyme type | coordinates of N-terminal alpha carbon of cystine pair | | | dist from origin (Å) |
|---|---|---|---|---|
| | x | y | z | |
| Influenza N2 | 33.5 | 19.4 | 7.4 | 39.4 |
| Influenza N9 | 34.4 | 18.3 | 8.0 | 39.8 |
| Influenza B (Lee) | 37.0 | 15.4 | 10.8 | 41.5 |
| Human Parainfluenza virus-3 | 32.3 | 31.6 | -1.7 | 45.3 |

## APPENDIX 1: NATURAL SELECTION AND SYMMETRY

The search of candidate quaternary structures was narrowed by consideration of the principle of Natural Selection and its corollary; that identical complex biological structures are likely to function in identical environments. In a tetrahedral arrangement, each subunit forms an interface with each of the three other subunits, and the only tetrahedral arrangements providing an identical environment for the four identical subunits require each of the three faces of a subunit to interact with the equivalent face on the neighbouring subunit. That is, each face must be self-complementary. Thus the most probable arrangements will have three perpendicular two-fold axes of symmetry, or D2 symmetry.

## APPENDIX 2: NATURAL SELECTION AND TETHER LOCATION

The neuraminidases of virus particles are necessarily tethered to the virus surface. The enzyme molecules would have some freedom of movement to enhance encounter with substrate but a virus particle having no protein synthesis capability cannot allow its enzymes to diffuse away. The tether is often described as a stalk and is found at the N-terminal end of the neuraminidase protein chain (17, 19). The tether must be attached to the main body of the enzyme by one or more strong interactions in addition to the main chain peptide bond or else the main chain could begin to unravel as the enzyme tended to move away from the virus through interactions with the environment, such as diffusion or adhesion. Identification of this point of attachment in crystal structures has to be partly subjective, since the C-terminal end of the tether could have a fixed position in crystals and appear to be part of the main body of the enzyme. Fortunately, most viral neuraminidases appear to use a disulfide linkage as the point of attachment of the tether. For example, the stalk or tether of N2 and N9 influenza neuraminidase can be described as extending from the N-terminal membrane anchor sequence, residues 7 to 35 (19), to residue 91. In the crystal, there are non-bonding contacts between the tether and the body of the enzyme at most of the residues from 82 to 91 but none of these is considered extensive or permanent enough to be regarded as the point of attachment. Cys92 is joined by a disulfide bond to a chain embedded in the body of the enzyme and is the first amino acid, starting from the N-terminal, to be unambiguously part of the body of the enzyme.

It is considered most probable that Natural Selection would have provided an attachment point such as to minimize the number of amino acids used in chain synthesis for a given effective chain length. For a tetrahedral structure with D2 symmetry, the optimum attachment points would be on a plane parallel to the surface of the virus and passing through the center of the tetramer. Only these points of attachment would allow a minimum number of amino acids to provide a given distance between the enzyme and the virus surface. D2 symmetry requires that this plane contains two of the rotational symmetry axes. A further requirement, if the number of amino acids is to be minimized, is that the tether should be able to extend in an approximately straight line from the enzyme to the virus surface. This requires that the points of attachment be close to the outer perimeter of the tetramer so that the tether is not substantially deflected by the body of the enzyme. Of course, thermal motion would mean that the four tethers would seldom be fully extended, but whatever the degree of extension, the points of attachment described above would minimize the number of amino acids required in the tether.

Don Vanselow

Don Vanselow

**APPENDIX 3: TRANSFORMATIONS TO GENERATE CHAIN A OF A TETRAHEDRON**

| Source species | File name | Move origin to:- (Å) | Then rotate molecule with:- | Ref |
|---|---|---|---|---|
| Influenza N2 | 1NN2.pdb | $\begin{bmatrix} 87.341 \\ 109.743 \\ 77.435 \end{bmatrix}$ | $\begin{bmatrix} -0.800 & -0.100 & -0.592 \\ 0.581 & 0.120 & -0.805 \\ 0.151 & -0.987 & -0.038 \end{bmatrix}$ | (4) |
| Influenza N9 | 7NN9.pdb | $\begin{bmatrix} 24.239 \\ 35.541 \\ 77.342 \end{bmatrix}$ | $\begin{bmatrix} -0.785 & 0.111 & -0.610 \\ 0.619 & 0.072 & -0.783 \\ -0.043 & -0.991 & -0.125 \end{bmatrix}$ | (27) |
| Influenza B (Lee) | 1INF.pdb | $\begin{bmatrix} 26.570 \\ -31.409 \\ 74.951 \end{bmatrix}$ | $\begin{bmatrix} 0.776 & -0.203 & -0.597 \\ -0.571 & 0.176 & -0.802 \\ 0.268 & 0.963 & 0.020 \end{bmatrix}$ | (15) |
| Human Parainfluenza virus-3 | 1V3B.pdb Chain A | $\begin{bmatrix} 46.382 \\ 146.692 \\ 10.036 \end{bmatrix}$ | $\begin{bmatrix} -0.488 & -0.723 & 0.488 \\ -0.368 & -0.337 & -0.867 \\ 0.791 & -0.603 & -0.102 \end{bmatrix}$ | (16) |
| Simian Parainfluenza virus-5 | 1Z4V.pdb | $\begin{bmatrix} 145.066 \\ -62.597 \\ -145.131 \end{bmatrix}$ | $\begin{bmatrix} 0.044 & 0.774 & 0.632 \\ 0.915 & 0.223 & -0.337 \\ -0.402 & 0.593 & -0.698 \end{bmatrix}$ | (17) |
| Newcastle disease virus | 1USR.pdb Chain A | $\begin{bmatrix} 124.351 \\ 41.888 \\ 68.583 \end{bmatrix}$ | $\begin{bmatrix} -0.348 & 0.451 & -0.822 \\ 0.625 & -0.542 & -0.562 \\ -0.699 & -0.709 & -0.093 \end{bmatrix}$ | (28) |
| Salmonella typhimurium | 2SIL.pdb | $\begin{bmatrix} 24.560 \\ 64.413 \\ 38.954 \end{bmatrix}$ | $\begin{bmatrix} -0.524 & -0.720 & 0.455 \\ 0.369 & -0.674 & -0.640 \\ 0.768 & -0.168 & 0.619 \end{bmatrix}$ | (29) |
| Vibrio cholerae | 1KIT.pdb | $\begin{bmatrix} 11.128 \\ 67.782 \\ 96.208 \end{bmatrix}$ | $\begin{bmatrix} 0.982 & 0.186 & 0.024 \\ 0.172 & -0.947 & 0.271 \\ 0.073 & -0.262 & -0.962 \end{bmatrix}$ | (30) |
| Micromonospora viridifaciens. | 1W8N.pdb | $\begin{bmatrix} 46.088 \\ 34.726 \\ 10.427 \end{bmatrix}$ | $\begin{bmatrix} 0.220 & -0.076 & 0.973 \\ -0.276 & 0.951 & 0.137 \\ -0.936 & -0.299 & 0.188 \end{bmatrix}$ | (31) |
| Leech | 1SLL.pdb | $\begin{bmatrix} -15.821 \\ -2.099 \\ 27.818 \end{bmatrix}$ | $\begin{bmatrix} 0.698 & 0.049 & -0.715 \\ 0.052 & 0.992 & 0.118 \\ 0.714 & -0.119 & 0.690 \end{bmatrix}$ | (32) |
| Human | 1SNT.pdb | $\begin{bmatrix} 16.848 \\ 17.794 \\ 30.732 \end{bmatrix}$ | $\begin{bmatrix} -0.360 & 0.887 & 0.289 \\ -0.816 & -0.149 & -0.559 \\ -0.453 & -0.437 & 0.777 \end{bmatrix}$ | (6) |

Fig 1. Tetramer of N9-type subunits, viewed down the y axis. Cys92 residues, coloured black and marked by arrows, lie close to the xy plane, indicated by the horizontal line. The figure was produced using RASMOL (8)

Fig 2. Tetramer of N9-type subunits viewed down the z axis. The self-complementarity of the two foreground subunits can be seen in the curved interface near the center of the figure. The figure was produced using RASMOL (8).

Fig 3. Tetramer of Micromonospora subunits viewed down the z axis. Two propeller domains can be seen docked with each other in the center. The attached C-terminal domains wrap around to dock with the symmetry-related propeller domain. The figure was produced using RASMOL (8).

Fig 4. Tetramer of Micromonospora subunits viewed down the x axis. This view again shows the high quality of docking. The figure was produced using RASMOL (8).

Fig 5. Effect of rotation about the propeller axis on steric clashes in three types of neuraminidase. In each case the upper curve shows numbers of atoms per subunit clashing with atoms of any kind in another subunit. The lower curves show numbers of backbone atoms clashing with other backbone atoms. The horizontal scale is in degrees of clockwise rotation viewed towards the center of the tetrahedron.

Fig 6. Dependence of buried surface areas on probe radius, for square and tetrahedral tetramers of N2 and N9 neuraminidase.

Fig 7. Map of the subunit interface of N2 neuraminidase in the proposed native tetrahedral arrangement. The interface consists of 3 planes that form the sides of an irregular trigonal pyramid, the edges of which are marked by the pseudo-threefold axes of the tetrahedron in directions marked on the figure. The centers of the planes are the x, y and z axes. The circled atom on the edge of the AD face is the amide nitrogen of Asn146, a site of glycosylation. The outlined group of residues on the AD face is the knob of large amino acids numbered 430-437. The adjacent blank area in the AD face is the depression and cleft where catalysis is thought to occur. A disaccharide molecule in darker shading is included on the pseudo-threefold axis between the AD and AC faces where a channel appears to provide for substrate to penetrate into the catalytic cleft. The locations of charged groups are marked and identified.

Don Vanselow

**Figure 1**

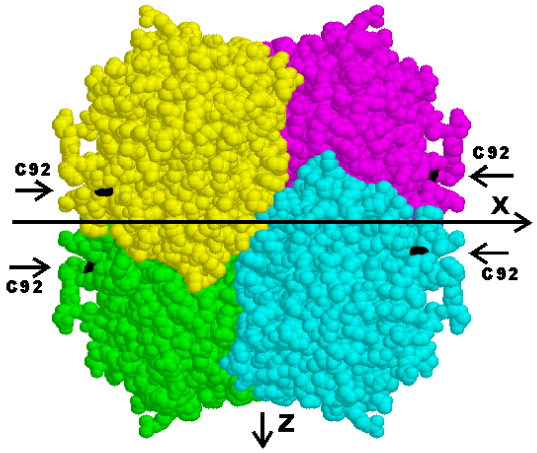


**Figure 2**

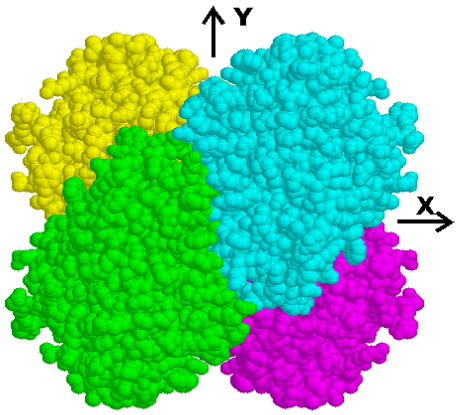

Don Vanselow

**Figure 3**

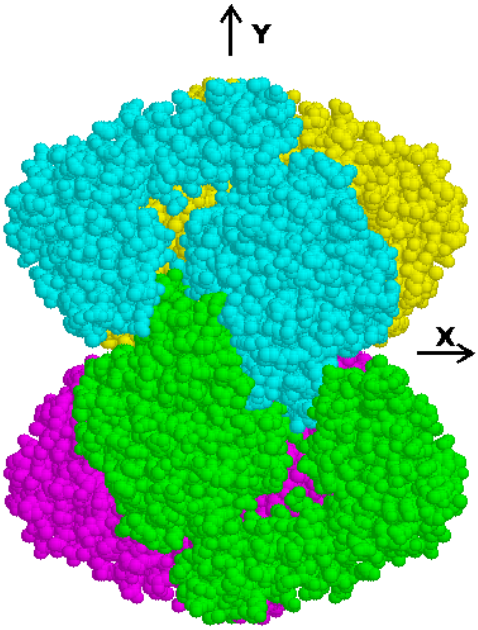


**Figure 4**

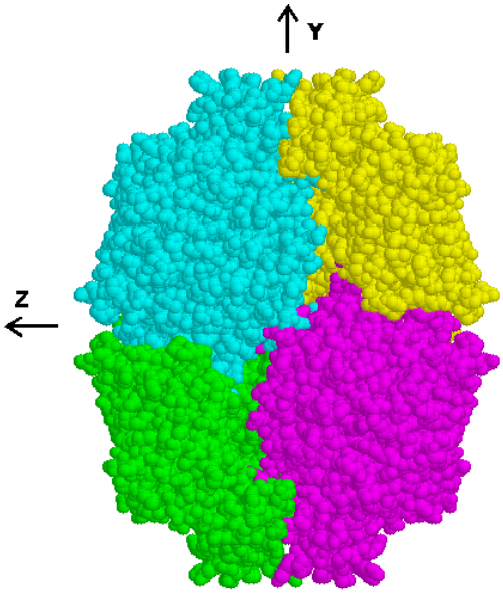

**Figure 5**

**Steric clashes per subunit versus angle of rotation about propeller axis. Upper curves are all atoms; lower curves are backbone atoms.**

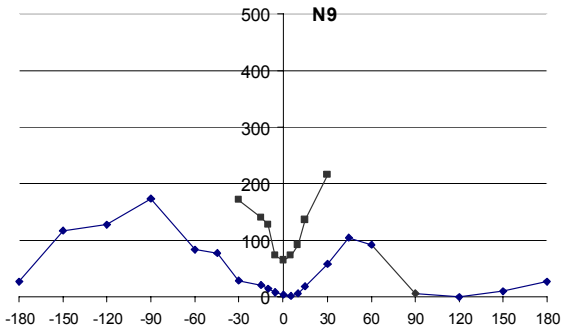


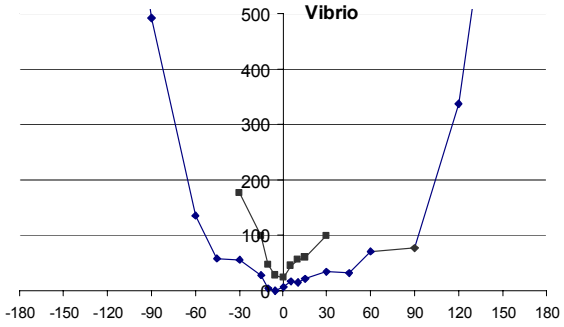


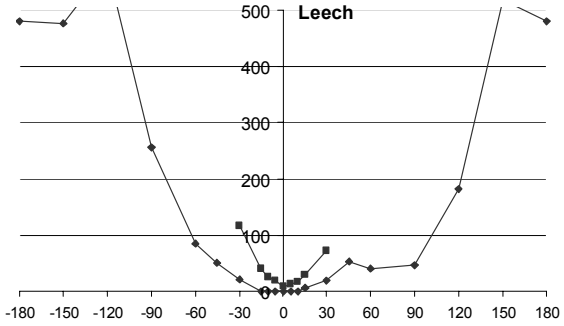

**Figure 6**

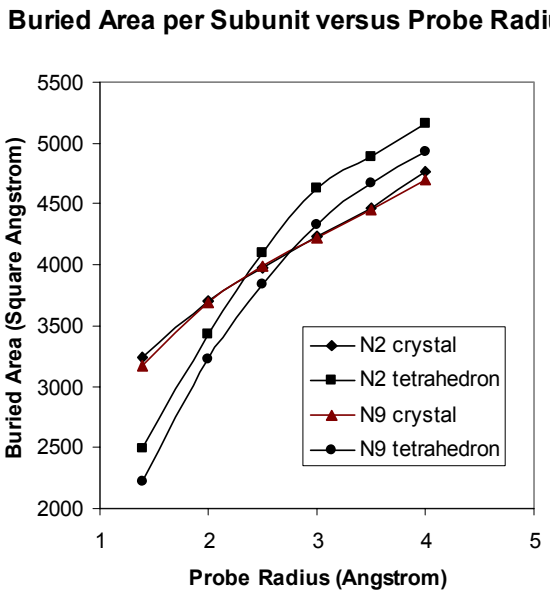
Buried Area per Subunit versus Probe Radius
Buried Area (Square Angstrom)
5500
5000
4500
4000
3500
3000
2500
2000
1
2
3
4
5
Probe Radius (Angstrom)
N2 crystal
N2 tetrahedron
N9 crystal
N9 tetrahedron

Don Vanselow

**Figure 7**